6-10-2014

Broadband, Non-destructive Characterisation of PEC-backed Materials Using a Dual-ridged-waveguide Probe

Milo W. Hyde IV
Air Force Institute of Technology

Michael J. Havrilla
Air Force Institute of Technology

Recommended Citation

Hyde, M. W., & Havrilla, M. J. (2015). Broadband, non-destructive characterisation of PEC-backed materials using a dual-ridged-waveguide probe. IET Science, Measurement & Technology, 9(1), 56–62. https://doi.org/10.1049/iet-smt.2013.0128

www.ietdl.org

Published in IET Science, Measurement and Technology
Received on 30th July 2013
Revised on 22nd April 2014
Accepted on 12th May 2014
doi: 10.1049/iet-smt.2013.0128

ISSN 1751-8822

Broadband, non-destructive characterisation of PEC-backed materials using a dual-ridged-waveguide probe

Milo W. Hyde IV, Michael J. Havrilla

Department of Electrical and Computer Engineering, Air Force Institute of Technology, Wright-Patterson AFB, OH, 45433, USA
E-mail: milo.hyde@afit.edu

Abstract: A new probe which utilises a dual-ridged waveguide to provide broadband, non-destructive (ND) material characterisation measurements of a perfect electric conductor (PEC)-backed material is introduced. The new probe possesses a bandwidth similar to existing coaxial probes and is structurally robust like rectangular waveguide probes. The combinations of these two qualities make it especially attractive for ND inspection/evaluation applications in the field. The theoretical development of the dual-ridged-waveguide probe is discussed. A magnetic field integral equation is derived by applying Love's equivalence theorem and enforcing the continuity of transverse fields at the dual-ridged-waveguide aperture. The magnetic field integral equation is then solved for the theoretical reflection coefficient using the method of moments. The permittivity and permeability of the material under test are found by minimising the root-mean-square difference between the theoretical and measured reflection coefficients using non-linear least squares. To validate the new probe, experimental results are presented of a magnetic absorbing material comparing results obtained using the new probe with those obtained using a traditional, destructive technique. The probe's sensitivity to sample thickness, flange-plate thickness, cutoff wavenumber and measured S-parameter uncertainties is also investigated.

1 Introduction

Waveguide probes have been used for non-destructive (ND) material characterisation applications with great success for over 30 years. Although some two-port waveguide probes have been developed [1–5], a majority of the published waveguide probe research deals with one-port or single-probe geometries because of their more widespread applicability [6–24]. Both coaxial [7, 10–12, 15, 18, 19, 21, 24] and rectangular/circular [6, 8, 9, 13, 14, 16, 17, 20, 22, 23] waveguide probes have been developed. The main advantage of using a coaxial probe is the potential for broadband material characterisation measurements; however, utilising coaxial probes for this purpose is difficult. In general, small aperture coaxial probes are most effective when used to characterise high-loss materials. Biological materials are often discussed in the literature, whose loss is driven by water content [19, 25–30]. On the other hand, large aperture probes are required to measure low-loss materials [10, 11]. This implies that broadband measurements using coaxial probes are only possible when the material under test (MUT) is known a priori to possess high loss. Rectangular/circular waveguide probes do not suffer from the coaxial probe problem just described and are more structurally robust than their coaxial counterparts making them especially useful for ND measurements in the field; however, they are naturally bandlimited.

In this paper, a new one-port waveguide probe is introduced which utilises a dual-ridged waveguide (DRWG) to provide ND, broadband (much like coaxial probes) material characterisation measurements of PEC-backed MUTs while maintaining the structural robustness of rectangular/circular waveguide probes. A schematic of the measurement geometry is shown in Fig. 1 – a DRWG attached to an infinite PEC flange plate is placed in contact with a PEC-backed magnetic material of unknown complex relative permittivity ε_r and permeability μ_r.

In the next section, the theoretical expression for the reflection coefficient S_{11}^{thy}, necessary to characterise the MUT, is derived. This is achieved by replacing the DRWG aperture with an equivalent magnetic current which maintains the fields in the parallel-plate/MUT region in accordance with Love's equivalence theorem [31–34]. Enforcing the continuity of the transverse magnetic fields at the DRWG aperture results in a magnetic field integral equation (MFIE), which when solved using the method of moments (MoM) [34, 35], yields S_{11}^{thy}. The ε_r and μ_r of the MUT are then found by minimising the root-mean-square difference between the theoretical $\boldsymbol{S}_{11}^{\text{thy}}$ and measured $\boldsymbol{S}_{11}^{\text{meas}}$ reflection coefficients using the trust-region-reflective method [36] subject to the constraints for passive materials, viz.

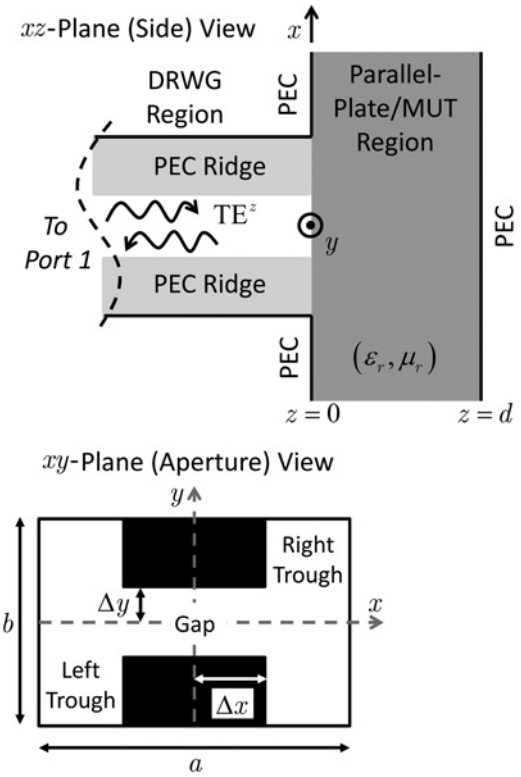

Fig. 1 *Single DRWG probe measurement geometry*

The top and bottom figures show the *xz*-plane (side) and *xy*-plane (aperture) views of the probe geometry, respectively

In the *xz*-plane view, the parallel-plate/MUT region is filled with the MUT (thickness d) of unknown complex relative permittivity ε_r and permeability μ_r

The DRWG region is free-space filled

In the *xy*-plane view, the DRWG sub regions (the gap, left trough and right trough) are labelled for the reader's convenience

$$\begin{pmatrix} \hat{\varepsilon}_r \\ \hat{\mu}_r \end{pmatrix} = \underset{\varepsilon_r,\,\mu_r \in \mathbb{C}}{\operatorname{argmin}} \left\| \boldsymbol{S}_{11}^{\text{thy}}(f;\,\varepsilon_r,\,\mu_r) - \boldsymbol{S}_{11}^{\text{meas}}(f) \right\|_2 \quad \begin{aligned} &\operatorname{Re}(\varepsilon_r) > 0, \quad \operatorname{Im}(\varepsilon_r) < 0 \\ &\operatorname{Re}(\mu_r) > 0, \quad \operatorname{Im}(\mu_r) < 0 \end{aligned} \tag{1}$$

where $\boldsymbol{S}_{11} = (S_{11,\,1},\, S_{11,\,2},\, \ldots,\, S_{11,\,n})^{\mathrm{T}}$ and f is the frequency.

At a minimum, $n = 2$ independent reflection measurements are required to unambiguously characterise the MUT. Several single-probe techniques have been developed to provide at least two independent reflection methods – most notably, two-layer method [16, 23, 37–39], two-iris method [40], frequency-varying method [16, 41], short/free-space-backed method [15, 23, 37] and two-thickness method [9, 16, 22, 42]. Of these, the two-layer and two-iris methods are the most universally applicable techniques for the ND characterisation of PEC backed MUTs. However, because of the analytical complexities involved in using the two-layer method (Green's function with off-diagonal elements combined with complex DRWG field expressions) and the additional hardware required to use the two-iris method, two-thickness method is utilised in this research. Note that this choice is only for convenience. Each of the techniques listed above can be used with the single DRWG probe presented in this paper.

Last, to experimentally verify the new probe, broadband material characterisation results of a magnetic absorbing material are presented and compared with those obtained using the traditional, destructive Nicolson–Ross–Weir (NRW) [43, 44] technique. The new probe's sensitivity to sample thickness, flange-plate thickness, cutoff wavenumber and measured S_{11} uncertainties is also presented.

2 Methodology

In this section, an expression for S_{11}^{thy} is derived for the single DRWG probe shown in Fig. 1. The forms of the fields in the DRWG and parallel-plate/MUT regions of the probe are detailed first. A MFIE is derived by enforcing the continuity of the transverse DRWG and parallel-plate/MUT region magnetic fields at the DRWG aperture, that is, $z = 0$. This MFIE is subsequently solved using the MoM.

2.1 DRWG and parallel-plate region field distributions

The fields in the DRWG region of Fig. 1 are found using the technique outlined by Montgomery [45] and later by Elliot [46]. First, the electric and magnetic fields in each DRWG subregion (i.e. the gap subregion, $|x| < \Delta x \cap |y| < \Delta y$, and the two trough subregions, $\Delta x < |x| < a/2 \cap |y| < b/2$) are expanded in a set of TE^z and, if applicable, TM^z modes [32]. Note that only the dominant DRWG mode, commonly termed a TE$^z_{10}$ hybrid mode [45, 47], is considered in this research. Thus, only the TE^z mode development is reported here.

The mode-matching technique [48] is then used to enforce the continuity of the transverse electric and magnetic fields at $x = -\Delta x$ and Δx producing the following homogeneous matrix equation

$$\boldsymbol{A}(k_{\text{c}}) \begin{pmatrix} \boldsymbol{\alpha} \\ \boldsymbol{\beta} \end{pmatrix} = \begin{pmatrix} \boldsymbol{A}^{11}(k_{\text{c}}) & \boldsymbol{A}^{12}(k_{\text{c}}) \\ \boldsymbol{A}^{21}(k_{\text{c}}) & \boldsymbol{A}^{22}(k_{\text{c}}) \end{pmatrix} \begin{pmatrix} \boldsymbol{\alpha} \\ \boldsymbol{\beta} \end{pmatrix} = 0 \tag{2}$$

where k_{c} is the cutoff wavenumber and $\boldsymbol{A}^{11}$, $\boldsymbol{A}^{12}$, $\boldsymbol{A}^{21}$ and $\boldsymbol{A}^{22}$ are $N \times N$ submatrices whose $\tilde{n}$th row and nth column entries are given by

$$\begin{aligned} A_{\tilde{n}n}^{11}(k_{\text{c}}) = A_{\tilde{n}n}^{22}(k_{\text{c}}) &= \frac{\tan\left(k_{x\tilde{n}}^{\text{g}}\Delta x\right) - \cot\left(k_{x\tilde{n}}^{\text{g}}\Delta x\right)}{2k_{x\tilde{n}}^{\text{g}}}\delta_{\tilde{n}n} \\ &\quad - \sum_m \frac{\psi_{mn}\psi_{m\tilde{n}}\cot\left[k_{xm}^{\text{t}}\left((a/2) - \Delta x\right)\right]}{k_{xm}^{\text{t}}(b/2)\left(1 + \delta_{m0}\right)\Delta y(1 + \delta_{\tilde{n}0})} \\ A_{\tilde{n}n}^{12}(k_{\text{c}}) = A_{\tilde{n}n}^{21}(k_{\text{c}}) &= \frac{\tan\left(k_{x\tilde{n}}^{\text{g}}\Delta x\right) - \cot\left(k_{x\tilde{n}}^{\text{g}}\Delta x\right)}{2k_{x\tilde{n}}^{\text{g}}}\delta_{\tilde{n}n} \end{aligned} \tag{3}$$

respectively. Here, n and $\tilde{n}$ represent basis and testing indices, respectively; δ_{ij} is the Kronecker delta; $k_{ym}^{\text{t}} = m\pi/b$ and $k_{yn}^{\text{g}} = n\pi/(2\Delta y)$ are the y-directed DRWG wavenumbers in the trough and gap subregions, respectively; $k_{xm}^{\text{t}} = \sqrt{k_{\text{c}}^2 - (k_{ym}^{\text{t}})^2}$ and $k_{xn}^{\text{g}} = \sqrt{k_{\text{c}}^2 - (k_{yn}^{\text{g}})^2}$ are the unknown x-directed DRWG wavenumbers in the trough and gap subregions, respectively; α_n and β_n are the unknown complex TE^z modal amplitudes; and

$$\begin{aligned} \psi_{mn} = \frac{1}{2}\left(\frac{1}{k_{yn}^{\text{g}} - k_{ym}^{\text{t}}} - \frac{1}{k_{yn}^{\text{g}} + k_{ym}^{\text{t}}}\right)\left\{\sin\left[k_{ym}^{\text{t}}\left(\frac{b}{2} - \Delta y\right)\right]\right. \\ \left. - (-1)^n \sin\left[k_{ym}^{\text{t}}\left(\frac{b}{2} + \Delta y\right)\right]\right\} \end{aligned} \tag{4}$$

The cutoff wavenumber k_{c} is found by forcing an eigenvalue

of $\boldsymbol{A}(k_c)$ to zero via numerical root search. The vector containing the complex modal amplitudes, $(\boldsymbol{\alpha}\ \boldsymbol{\beta})^T$, is the associated eigenvector of that zero eigenvalue. There are an infinite number of wavenumbers which satisfy (2) each corresponding to a distinct TE^z DRWG mode. The k_c which corresponds to the first zero of (2) is the dominant DRWG mode cutoff wavenumber.

After k_c and $(\boldsymbol{\alpha}\ \boldsymbol{\beta})^T$ have been found, expressions for the TE^z transverse DRWG fields can be obtained. The transverse fields in the DRWG region ($z<0$) are

$$\boldsymbol{E}_t = \left(e^{-jk_z z} + \Gamma e^{jk_z z}\right)\begin{cases} \boldsymbol{e}_t^g(\boldsymbol{\rho}) & |x|<\Delta x \\ \boldsymbol{e}_t^{lt}(\boldsymbol{\rho}) & x<-\Delta x \\ \boldsymbol{e}_t^{rt}(\boldsymbol{\rho}) & x>\Delta x \end{cases}$$
$$\boldsymbol{H}_t = \left(e^{-jk_z z} - \Gamma e^{jk_z z}\right)\begin{cases} \boldsymbol{h}_t^g(\boldsymbol{\rho}) & |x|<\Delta x \\ \boldsymbol{h}_t^{lt}(\boldsymbol{\rho}) & x<-\Delta x \\ \boldsymbol{h}_t^{rt}(\boldsymbol{\rho}) & x>\Delta x \end{cases} \tag{5}$$

Here $k_z = \sqrt{k_0^2 - k_c^2}$, where $k_0 = 2\pi f\sqrt{\varepsilon_0\mu_0}$; $\Gamma = S_{11}^{thy}$ is the desired theoretical reflection coefficient; and $\boldsymbol{e}_t^g$, $\boldsymbol{h}_t^g$, $\boldsymbol{e}_t^{extrt}$, $\boldsymbol{h}_t^{rt}$, $\boldsymbol{e}_t^{lt}$, and $\boldsymbol{h}_t^{lt}$ are the DRWG dominant-mode transverse electric and magnetic field distributions in the gap and trough subregions, respectively. The analytical forms for these field distributions can be found in [4] and are not provided here for the sake of brevity.

The transverse magnetic field in the parallel-plate/MUT region of Fig. 1 is found by replacing the DRWG aperture with an equivalent transverse magnetic current $\mathcal{M}$ in accordance with Love's equivalence theorem [31–34]. The transverse magnetic field is given by

$$\boldsymbol{H}_t^{pp}(\boldsymbol{\rho}, z) = \frac{1}{j\omega\mu\varepsilon}\left(\bar{\boldsymbol{I}}_t k^2 + \nabla_t\nabla\right)\cdot\boldsymbol{F}(\boldsymbol{\rho}, z) \tag{6}$$

where the electric vector potential $\boldsymbol{F}$ is

$$\boldsymbol{F}(\boldsymbol{\rho}, z) = \int\int_S \bar{\boldsymbol{G}}(\boldsymbol{\rho}, z|\boldsymbol{\rho}', 0)\cdot\varepsilon\mathcal{M}(\boldsymbol{\rho}')\,dS' \tag{7}$$

where $\bar{\boldsymbol{G}}$ is the dyadic magnetic-current-excited parallel-plate Green's function [49], $\bar{\boldsymbol{I}}_t = \hat{\boldsymbol{x}}\hat{\boldsymbol{x}} + \hat{\boldsymbol{y}}\hat{\boldsymbol{y}}$, $\nabla_t = \hat{\boldsymbol{x}}(\partial/\partial x) + \hat{\boldsymbol{y}}(\partial/\partial y)$, $\boldsymbol{\rho} = \hat{\boldsymbol{x}}x + \hat{\boldsymbol{y}}y$ is the observation vector, $\boldsymbol{\rho}' = \hat{\boldsymbol{x}}x' + \hat{\boldsymbol{y}}y'$ is the source vector, S represents the DRWG aperture cross section and $k = 2\pi f\sqrt{\varepsilon\mu}$.

2.2 MFIE and MoM solution

A MFIE can be derived by enforcing the continuity of the transverse magnetic fields in the DRWG and parallel-plate/MUT regions at $z=0$, namely

$$\frac{1}{j\omega\mu\varepsilon}(\bar{\boldsymbol{I}}_t k^2 + \nabla_t\nabla)\cdot\boldsymbol{F}(\boldsymbol{\rho}, 0)$$
$$= (1-\Gamma)\begin{cases} \boldsymbol{h}_t^g(\boldsymbol{\rho}) & |x|<\Delta x \\ \boldsymbol{h}_t^{lt}(\boldsymbol{\rho}) & x<-\Delta x \\ \boldsymbol{h}_t^{rt}(\boldsymbol{\rho}) & x>\Delta x \end{cases} \quad \boldsymbol{\rho}\in S \tag{8}$$

where the unknowns in the above MFIE are $\mathcal{M}$ and Γ. Expanding $\mathcal{M}$ using the transverse DRWG electric field distribution given in (5) and testing the resulting expression with the transverse DRWG magnetic field distribution also given in (5) yields the desired S_{11}^{thy}.

It is possible to calculate the convolution integral in (7) directly. This approach requires the numerical evaluation of four integrals – two basis and two testing integrals. It is numerically advantageous to apply the convolution theorem and perform the required integrations in the spectral domain [39]. This approach permits all the basis and testing integrals to be computed in closed form yielding spectral domain integrals which, in the worst computational cases, are given by

$$\sum_{n,m}\sum_{\tilde{n},\tilde{m}} e_{yn,m}^t e_{y\tilde{n},\tilde{m}}^t \int_{-\infty}^{\infty}(k^2-\xi^2) f_{m,\tilde{m}}(\xi) \int_{-\infty}^{\infty}\frac{\cosh(pd)}{p\sinh(pd)} g_{m,\tilde{m}}(\eta)\,d\eta\,d\xi \tag{9}$$

where $p = \sqrt{\xi^2+\eta^2-k^2}$ is the spectral domain wavenumber and

$$f_{m,\tilde{m}}(\xi) = \int_{\Delta x}^{a/2}\sin\left[k_{xm}^t\left(\frac{a}{2}-x'\right)\right]\cos(\xi x')\,dx' \times \int_{\Delta x}^{a/2}\sin\left[k_{x\tilde{m}}^t\left(\frac{a}{2}-x\right)\right]\cos(\xi x)\,dx$$
$$g_{m,\tilde{m}}(\eta) = \int_{-b/2}^{b/2}\cos\left[k_{ym}^t\left(y'-\frac{b}{2}\right)\right]e^{-j\eta y'}\,dy' \times \int_{-b/2}^{b/2}\cos\left[k_{y\tilde{m}}^t\left(y-\frac{b}{2}\right)\right]e^{j\eta y}\,dy \tag{10}$$

The η integral can be evaluated using complex-plane analysis yielding a pole-series representation. The remaining ξ integral contains irremovable branch cuts and is therefore most easily computed numerically [3, 5, 22].

It should be noted that because of the summations in the basis and testing functions, special care must be taken when computing the spectral domain integrals. For optimal computational efficiency, it is best to bring the summations inside the ξ integral, evaluate the η integral via complex-plane analysis, evaluate the resulting summations and lastly, calculate the ξ integral numerically. Note that there are a total of 16 distinct spectral domain integrals which must be evaluated.

3 Experimental verification

3.1 Apparatus description and experimental procedure

To validate the new ND broadband probe, material measurements were made of ECCOSORB® SF-3 ($d = 1.85$ mm) [50] using an Agilent E8362B vector network analyzer (VNA) [51]. The data were collected from 6 to 18 GHz using the apparatus shown in Fig. 2. The DRWG probe apparatus consisted of a single Microwave Engineering Corporation WRD650 DRWG ($a = 18.29$ mm, $b = 8.15$ mm, $\Delta x = 2.20$ mm and $\Delta y = 1.28$ mm) [52] connected via screws to a 15.24 cm × 15.24 cm × $h = 0.95$ cm aluminium flange plate. On the side of the flange plate which connected to the DRWG, 3.18 mm alignment holes were machined to ensure precision alignment between the DRWG and the flange-plate apertures.

Before the material measurements were made, the apparatus was calibrated using a thru-reflect-line (TRL) calibration [53]. Two custom made DRWG line standards

doi: 10.1049/iet-smt.2013.0128

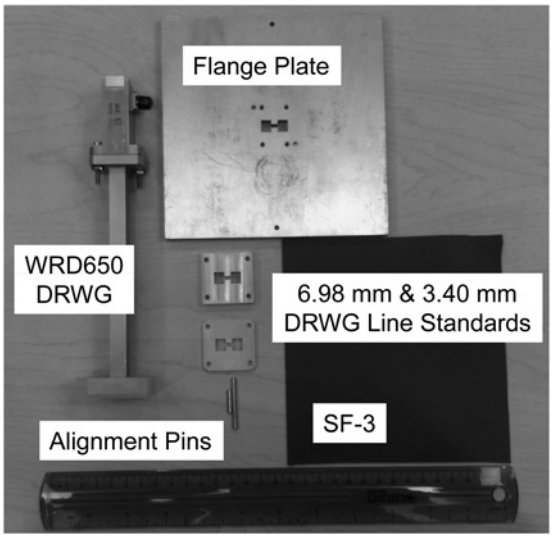

Fig. 2 *Photograph of the DRWG measurement apparatus with all parts labelled*

were used in the calibration – one 6.98 mm thick to cover 6–12 GHz and one 3.40 mm thick to cover 12–18 GHz. These line standards can be seen in the photograph in Fig. 2. The TRL calibration placed the port 1 calibration plane at the DRWG aperture. This calibration plane was then phase shifted to the front face of the MUT by

$$S_{11}^{\text{meas}} = S_{11}^{\text{TRL}} e^{2\text{j}k_z h} \tag{11}$$

The ε_r and μ_r of SF-3 were found by solving (1) to within a tolerance of 10^{-6} using the trust-region-reflective method [36]. As discussed above, two-thickness method [9, 16, 22, 42] was utilised to provide the second independent S_{11} measurement necessary to find ε_r and μ_r unambiguously. This method was chosen for analytical and computational convenience.

The new probe's sensitivity to measurement errors was also investigated. Uncertainty analysis was performed on the extracted ε_r and μ_r values taking into account errors in S_{11}^{meas} ($\sigma_{S_{11}}$ given in [51]), flange-plate thickness h ($\sigma_h = 0.05$ mm), MUT thickness d ($\sigma_{d1} = \sigma_{d2} = 0.05$ mm) and cutoff wavenumber k_{c} ($\sigma_{k_{\text{c}}} = 0.03k_{\text{c}}$). Note that $\sigma_{k_{\text{c}}}$ arises mainly from uncertainties in DRWG aperture dimensions, in particular, errors because of gap width Δx and gap height Δy as well as errors because of rounded aperture corners [54]. Recent work has shown that the value of k_{c} varies by approximately 3% when these factors are considered [54]. To the authors' knowledge, this is the first time that the effect of this error on the ε_r and μ_r extracted using a waveguide probe has been quantified.

One error source which was not considered in this analysis was probe lift-off or air-gap error [37]. To minimise the impact of this error, four vise-grip clamps were used to securely hold the flange plate, MUT and PEC-backing plate together. The clamps were placed surrounding and as close as possible to the DRWG aperture where the field concentration and therefore the impact of possible air gaps was the strongest. Quantifying probe lift-off error requires the two-layer magnetic-current-excited parallel-plate Green's function, which when combined with the complex analytical form of the DRWG fields, represents a significant theoretical and computational challenge beyond the scope of the work presented here. Quantifying probe lift-off error is therefore left to future work.

The following expression was used to calculate the measurement uncertainty in the real part of ε_r [55]

$$\begin{aligned}\sigma_{\varepsilon_r^{\text{r}}}^2 = &\left(\frac{\partial \varepsilon_r^{\text{r}}}{\partial S_{11,1}^{\text{r}}}\sigma_{S_{11,1}^{\text{r}}}\right)^2 + \left(\frac{\partial \varepsilon_r^{\text{r}}}{\partial S_{11,1}^{xti}}\sigma_{S_{11,1}^{\text{i}}}\right)^2 \\ &+ \left(\frac{\partial \varepsilon_r^{\text{r}}}{\partial S_{11,2}^{\text{r}}}\sigma_{S_{11,2}^{\text{r}}}\right)^2 + \left(\frac{\partial \varepsilon_r^{\text{r}}}{\partial S_{11,2}^{\text{i}}}\sigma_{S_{11,2}^{\text{i}}}\right)^2 \\ &+ \left(\frac{\partial \varepsilon_r^{\text{r}}}{\partial d_1}\sigma_{d_1}\right)^2 + \left(\frac{\partial \varepsilon_r^{\text{r}}}{\partial d_2}\sigma_{d_2}\right)^2 + \left(\frac{\partial \varepsilon_r^{\text{tr}}}{\partial h}\sigma_h\right)^2 \\ &+ \left(\frac{\partial \varepsilon_r^{\text{r}}}{\partial k_{\text{c}}}\sigma_{k_{\text{c}}}\right)^2\end{aligned} \tag{12}$$

where the superscripts 'r' and 'i' denote the real and imaginary parts and '11, 1' and '11, 2' denote the first and second S_{11} measurements (i.e. thickness 1 and thickness 2 mm), respectively. The partial derivatives in the above expression were estimated using the forward difference approximation. The values for $\sigma_{\varepsilon_r^{\text{i}}}$, $\sigma_{\mu_r^{\text{r}}}$ and $\sigma_{\mu_r^{\text{i}}}$ were calculated in a similar manner as above. Note that the error values provided by (12) are worst case estimates [55].

3.2 ECCOSORB® SF-3 results

Fig. 3 shows the SF-3 ε_r (Fig. 3*a*) and μ_r (Fig. 3*b*) results using the single DRWG probe (blue bars) introduced in this work. The solid black traces are the traditional, destructive NRW technique results using an SF-3 sample which uniformly fills the cross section of the DRWG. These results are provided to serve as a reference. Additional information about these DRWG NRW measurements, including descriptions of measurement procedures and sources of error, can be found in [54]. The widths of the blue bars in the plots represent the errors in ε_r and μ_r, that is, $\pm 2\sigma_{\varepsilon_r}$ and $\pm 2\sigma_{\mu_r}$, respectively, because of the measurement errors discussed above.

Overall, the SF-3 ε_r and μ_r reference results generally lie within the margins of error of the DRWG probe results. The major discrepancy between the two occurs in the μ_r^{i} results, where the DRWG probe overestimates the amount of magnetic loss. Although the quality of the DRWG probe μ_r^{i} estimate presented here is poor, it is consistent with those reported in the literature for similar ND single probe measurement geometries [15, 16, 22, 23, 38, 40–42].

3.3 Flange-plate size

Before concluding, it is worth discussing flange-plate size as this directly affects the probe's applicability for field measurements. Because of the possibility that reflections from the edges of the flange plate would corrupt the reflection measurements (recall that in the theoretical development, the flange plate is assumed to be infinite in extent), waveguide probes have traditionally been applied to lossy materials. In these cases, the flange plate needs to be large enough such that the unwanted edge reflected wave is attenuated to a degree less than the noise floor of the VNA. This condition is easily met for SF-3 and the 15.24 cm × 15.24 cm flange plate used in the experimental results discussed above. The traditional approach to determining

doi: 10.1049/iet-smt.2013.0128

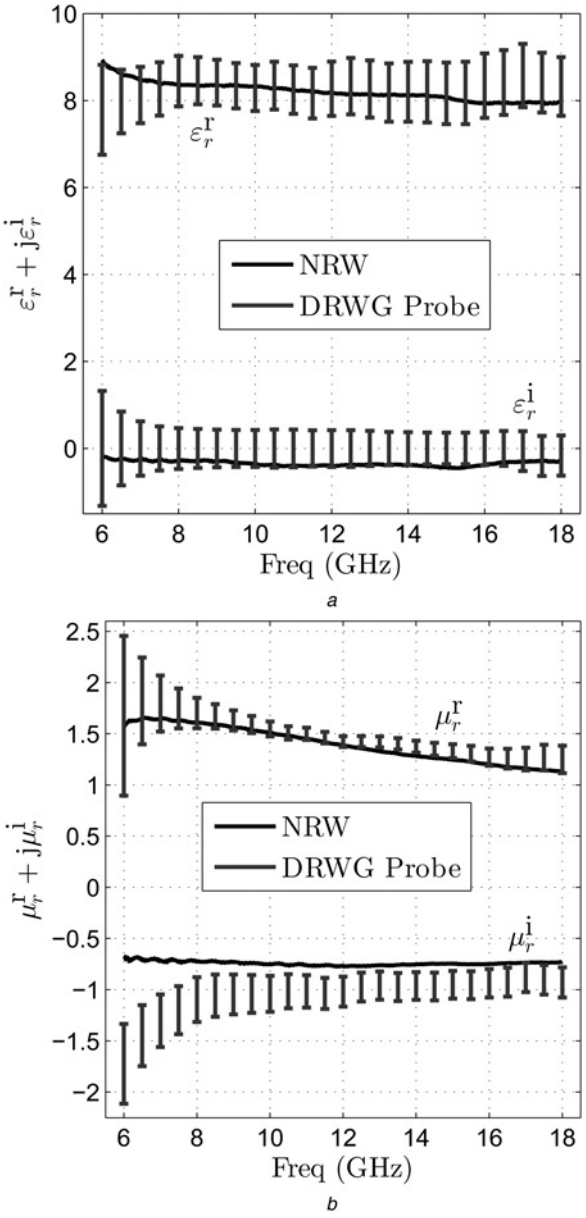

Fig. 3 *SF-3 ε_r and μ_r*

a Complex permittivity ε_r and
b Permeability μ_r results for SF-3 using two-thickness method and the single DRWG probe (bars) analysed in this work
The solid black traces are the traditional, destructive NRW technique results using an SF-3 sample which uniformly fills the cross section of the DRWG These results are provided to serve as a reference
The widths of the bars in the plots represent the errors in ε_r and μ_r ($\pm 2\sigma_{\varepsilon_r}$ and $\pm 2\sigma_{\mu_r}$) due to uncertainties in S_{11}^{meas} d, k_{c} and h

flange size works well when one knows that the MUT is lossy; however, it stipulates an unrealistic flange size when the MUT is low loss. A simple technique to overcome this limitation is to remove the unwanted edge reflections via time-domain gating the measured reflection coefficient [56]. To use this approach, the characterisation measurement must possess sufficient bandwidth such that the edge reflections can be resolved. This criterion is

$$B = \frac{c}{2\rho\sqrt{\varepsilon_r \mu_r}} \tag{13}$$

where B is the minimum required bandwidth, $c/\sqrt{\varepsilon_r \mu_r}$ is the speed of light in the MUT and ρ is the radius of the flange plate [56]. Solving (13) for ρ yields the minimum flange-plate radius in which the edge reflections can be resolved and thus removed via time-domain gating. Since a vast majority of materials at microwave frequencies possess slower phase velocities than c, (13) can still be used to determine an acceptable flange-plate size even if ε_r and μ_r are unknown by assuming the MUT is free space. Applying this criterion for the DRWG probe presented here results in a minimum flange-plate radius $\rho = 1.25$ cm. This is significantly smaller than that stipulated by the traditional flange-size calculation, in which the minimum flange-plate radius is approximately 3 m.

4 Conclusion

In this paper, a new waveguide probe which utilised a DRWG to provide broadband, ND material characterisation results of PEC-backed materials was introduced. The new probe possessed two qualities – broad bandwidth similar to coaxial probes and structure robustness characteristic of rectangular waveguide probes – which made it especially attractive for NDI/NDE applications in the field. The theoretical development of the DRWG probe was discussed in Section 2. This involved the derivation of the theoretical reflection coefficient necessary to characterise the MUT. This was achieved by utilising Love's equivalence theorem to replace the DRWG aperture with an equivalent magnetic current. The continuity of transverse magnetic fields at the DRWG aperture was then enforced yielding a MFIE, which was subsequently solved for the theoretical reflection coefficient using the MoM. The ε_r and μ_r of the MUT were then found by minimising the root-mean-square difference between the theoretical and measured reflection coefficients using the trust-region-reflective method. To experimentally verify the new probe, material characterisation results of ECCOSORB® SF-3 were presented and compared with those obtained using the traditional, destructive NRW technique. The probe's sensitivity to sample thickness, flange-plate thickness, cutoff wavenumber and measured reflection coefficient uncertainties was also discussed. It was observed that the $\varepsilon_r^{\mathrm{r}}$, $\varepsilon_r^{\mathrm{i}}$ and μ_r^{r} values returned by the probe were consistent with the reference results; however, there was a significant discrepancy between the probe and reference μ_r^{i} results. Although the new probe performed poorly in this regard, μ_r^{i} results of this quality are reported elsewhere in the literature for similar ND single probe measurement geometries. It should be noted that in the analysis presented here, only the contribution from the dominant DRWG mode was considered because of the theoretical and computational complexity of the problem. Incorporating higher-order DRWG modes into the analysis is future work.

5 Acknowledgments

The views expressed in this paper are those of the authors and do not reflect the official policy or position of the U.S. Air Force, the Department of Defense, or the U.S. Government.

6 References

1 Baker-Jarvis, J., Janezic, M.D.: 'Analysis of a two-port flanged coaxial holder for shielding effectiveness and dielectric measurements of thin films and thin materials', *IEEE Trans. Electromagn. Compat.*, 1996, **38**, (1), pp. 67–70

doi: 10.1049/iet-smt.2013.0128

2 Bird, T.: 'Mutual coupling in arrays of coaxial waveguides and horns', *IEEE Trans. Antennas Propag.*, 2004, **52**, (3), pp. 821–829
3 Hyde, M.W., Havrilla, M.J.: 'A nondestructive technique for determining complex permittivity and permeability of magnetic sheet materials using two flanged rectangular waveguides', *PIER*, 2008, **79**, pp. 367–386
4 Hyde, M.W., Havrilla, M.J.: 'A clamped dual-ridged waveguide measurement system for the broadband, nondestructive characterization of sheet materials', *Radio Sci.*, 2013, **48**, (5), pp. 628–637, URL http://www.dx.doi.org/10.1002/rds.20044
5 Hyde, M.W., Stewart, J.W., Havrilla, M.J., Baker, W.P., Rothwell, E.J., Nyquist, D.P.: 'Nondestructive electromagnetic material characterization using a dual waveguide probe: a full wave solution', *Radio Sci.*, 2009, **44**, (3), pp. RS3013, URL http://www.dx.doi.org/10.1029/2008RS003937
6 Bois, K.J., Benally, A., Zoughi, R.: 'Multimode solution for the reflection properties of an open-ended rectangular waveguide radiating into a dielectric half-space: the forward and inverse problems', *IEEE Trans. Instrum. Meas.*, 1999, **48**, (6), pp. 1131–1140
7 Boybay, M.S., Ramahi, O.M.: 'Open-ended coaxial line probes with negative permittivity materials', *IEEE Trans. Antennas Propag.*, 2011, **59**, (5), pp. 1765–1769
8 Chang, C.-W., Chen, K.-M., Qian, J.: 'Nondestructive measurements of complex tensor permittivity of anisotropic materials using a waveguide probe system', *IEEE Trans. Microw. Theory Tech.*, 1996, **44**, (7), pp. 1081–1090
9 Chang, C.-W., Chen, K.-M., Qian, J.: 'Nondestructive determination of electromagnetic parameters of dielectric materials at X-band frequencies using a waveguide probe system', *IEEE Trans. Instrum. Meas.*, 1997, **46**, (5), pp. 1084–1092
10 De Langhe, P., Blomme, K., Martens, L., De Zutter, D.: 'Measurement of low-permittivity materials based on a spectral-domain analysis for the open-ended coaxial probe', *IEEE Trans. Instrum. Meas.*, 1993, **42**, (5), pp. 879–886
11 De Langhe, P., Martens, L., De Zutter, D.: 'Design rules for an experimental setup using an open-ended coaxial probe based on theoretical modelling', *IEEE Trans. Instrum. Meas.*, 1994, **43**, (6), pp. 810–817
12 Folgerø, K., Tjomsland, T.: 'Permittivity measurement of thin liquid layers using open-ended coaxial probes', *Meas. Sci. Technol.*, 1996, **7**, (8), pp. 1164–1173, URL http://www.stacks.iop.org/0957-0233/7/i=8/a=012
13 Ganchev, S.I., Bakhtiari, S., Zoughi, R.: 'A novel numerical technique for dielectric measurement of generally lossy dielectrics', *IEEE Trans. Instrum. Meas.*, 1992, **41**, (3), pp. 361–365
14 Huber, C., Abiri, H., Ganchev, S.I., Zoughi, R.: 'Modeling of surface hairline-crack detection in metals under coatings using an open-ended rectangular waveguide', *IEEE Trans. Microw. Theory Tech.*, 1997, **45**, (11), pp. 2049–2057
15 Li, C.-L., Chen, K.-M.: 'Determination of electromagnetic properties of materials using flanged open-ended coaxial probe – full-wave analysis', *IEEE Trans. Instrum. Meas.*, 1995, **44**, (1), pp. 19–27
16 Maode, N., Yong, S., Jinkui, Y., Chenpeng, F., Deming, X.: 'An improved open-ended waveguide measurement technique on parameters ε_r and μ_r of high-loss materials', *IEEE Trans. Instrum. Meas.*, 1998, **47**, (2), pp. 476–481
17 Mazlumi, F., Sadeghi, S.H.H., Moini, R.: 'Interaction of an open-ended rectangular waveguide probe with an arbitrary-shape surface crack in a lossy conductor', *IEEE Trans. Microw. Theory Tech.*, 2006, **54**, (10), pp. 3706–3711
18 Olmi, R., Bini, M., Nesti, R., Pelosi, G., Riminesi, C.: 'Improvement of the permittivity measurement by a 3D full-wave analysis of a finite flanged coaxial probe', *J. Electromagn. Waves Appl.*, 2004, **18**, pp. 217–232, URL http://www.ingentaconnect.com/content/vsp/jew/2004/00000018/00000002/art00011
19 Popovic, D., McCartney, L., Beasley, C., *et al.*: 'Precision open-ended coaxial probes for *in vivo* and *ex vivo* dielectric spectroscopy of biological tissues at microwave frequencies', *IEEE Trans. Microw. Theory Tech.*, 2005, **53**, (5), pp. 1713–1722
20 Sanadiki, B., Mostafavi, M.: 'Inversion of inhomogeneous continuously varying dielectric profiles using open-ended waveguides', *IEEE Trans. Antennas Propag.*, 1991, **39**, (2), pp. 158–163
21 Shin, D.H., Eom, H.J.: 'Estimation of dielectric slab permittivity using a flared coaxial line', *Radio Sci.*, 2003, **38**, (2), pp. 1034–1043
22 Stewart, J.W., Havrilla, M.J.: 'Electromagnetic characterization of a magnetic material using an open-ended waveguide probe and a rigorous full-wave multimode model', *J. Electromagn. Waves Appl.*, 2006, **20**, pp. 2037–2052, URL http://www.ingentaconnect.com/content/vsp/jew/2006/00000020/00000014/art00013
23 Tantot, O., Chatard-Moulin, M., Guillon, P.: 'Measurement of complex permittivity and permeability and thickness of multilayered medium by an open-ended waveguide method', *IEEE Trans. Instrum. Meas.*, 1997, **46**, (2), pp. 519–522
24 Wu, M., Yao, X., Zhang, L.: 'An improved coaxial probe technique for measuring microwave permittivity of thin dielectric materials', *Meas. Sci. Technol.*, 2000, **11**, (11), pp. 1617–1622, URL http://stacks.iop.org/0957-0233/11/i=11/a=311
25 Athey, T., Stuchly, M., Stuchly, S.: 'Measurement of radio frequency permittivity of biological tissues with an open-ended coaxial line: Part I', *IEEE Trans. Microw. Theory Tech.*, 1982, **30**, (1), pp. 82–86
26 Gajda, G., Stuchly, S.: 'Numerical analysis of open-ended coaxial lines', *IEEE Trans. Microw. Theory Tech.*, 1983, **31**, (5), pp. 380–384
27 Li, L., Ismail, N., Taylor, L., Davis, C.: 'Flanged coaxial microwave probes for measuring thin moisture layers', *IEEE Trans. Biomed. Eng.*, 1992, **39**, (1), pp. 49–57
28 Stuchly, M.A., Stuchly, S.S.: 'Coaxial line reflection methods for measuring dielectric properties of biological substances at radio and microwave frequencies-a review', *IEEE Trans. Instrum. Meas.*, 1980, **29**, (3), pp. 176–183
29 Stuchly, M., Athey, T., Samaras, G., Taylor, G.: 'Measurement of radio frequency permittivity of biological tissues with an open-ended coaxial line: Part II – experimental results', *IEEE Trans. Microw. Theory Tech.*, 1982, **30**, (1), pp. 87–92
30 Xu, D., Liu, L., Jiang, Z.: 'Measurement of the dielectric properties of biological substances using an improved open-ended coaxial line resonator method', *IEEE Trans. Microw. Theory Tech.*, 1987, **35**, (12), pp. 1424–1428
31 Chen, K.-M.: 'A mathematical formulation of the equivalence principle', *IEEE Trans. Microw. Theory Tech.*, 1989, **37**, (10), pp. 1576–1581
32 Collin, R.E.: 'Field Theory of Guided Waves' (IEEE Press, New York, NY, 1991, 2nd edn.)
33 Harrington, R.: 'Time-Harmonic Electromagnetic Fields' (IEEE Press, 2001)
34 Peterson, A.F., Ray, S.L., Mittra, R.: 'Computational Methods for Electromagnetics' (IEEE Press, New York, NY, 1998)
35 Harrington, R.: 'Field Computation by Moment Methods' (IEEE Press, New York, NY, 1993)
36 Coleman, T., Li, Y.: 'An interior trust region approach for nonlinear minimization subject to bounds', *SIAM J. Optim.*, 1996, **6**, (2), pp. 418–445, URL http://www.epubs.siam.org/doi/abs/10.1137/0806023
37 Baker-Jarvis, J., Janezic, M.D., Domich, P.D., Geyer, R.G.: 'Analysis of an open-ended coaxial probe with lift-off for nondestructive testing', *IEEE Trans. Instrum. Meas.*, 1994, **43**, (5), pp. 711–718
38 Dester, G.D., Rothwell, E.J., Havrilla, M.J., Hyde, M.W.: 'Error analysis of a two-layer method for the electromagnetic characterization of conductor-backed absorbing material using an open-ended waveguide probe', *PIER B*, 2010, **26**, pp. 1–21
39 Hyde, M., Havrilla, M., Bogle, A., Rothwell, E., Dester, G.: 'An improved two-layer method for nondestructively characterizing magnetic sheet materials using a single rectangular waveguide probe', *Electromagnetics*, 2012, **32**, (7), pp. 411–425, URL http://www.dx.doi.org/10.1080/02726343.2012.716702
40 Dester, G.D., Rothwell, E.J., Havrilla, M.J.: 'Two-iris method for the electromagnetic characterization of conductor-backed absorbing materials using an open-ended waveguide probe', *IEEE Trans. Instrum. Meas.*, 2012, **61**, (4), pp. 1037–1044
41 Wang, S., Niu, M., Xu, D.: 'A frequency-varying method for simultaneous measurement of complex permittivity and permeability with an open-ended coaxial probe', *IEEE Trans. Microw. Theory Tech.*, 1998, **46**, (12), pp. 2145–2147
42 Chen, C.-P., Ma, Z., Anada, T., Hsu, J.-P.: 'Further study on two-thickness-method for simultaneous measurement of complex EM parameters based on open-ended coaxial probe'. Proc. of the European Microwave Conf., October 2005
43 Nicolson, A.M., Ross, G.F.: 'Measurement of the intrinsic properties of materials by time-domain techniques', *IEEE Trans. Instrum. Meas.*, 1970, **19**, (4), pp. 377–382
44 Weir, W.B.: 'Automatic measurement of complex dielectric constant and permeability at microwave frequencies', *Proc. IEEE*, 1974, **62**, (1), pp. 33–36
45 Montgomery, J.: 'On the complete eigenvalue solution of ridged waveguide', *IEEE Trans. Microw. Theory Tech.*, 1971, **19**, (6), pp. 547–555
46 Elliot, R.S.: 'An Introduction to Guided Waves and Microwave Circuits' (Prentice-Hall, Inc., Englewood Cliffs, NJ, 1993)
47 Sun, W., Balanis, C.: 'MFIE analysis and design of ridged waveguides', *IEEE Trans. Microw. Theory Tech.*, 1993, **41**, (11), pp. 1965–1971
48 Wexler, A.: 'Solution of waveguide discontinuities by modal analysis', *IEEE Trans. Microw. Theory Tech.*, 1967, **15**, (9), pp. 508–517
49 Hanson, G.W., Yakovlev, A.B.: 'Operator Theory for Electromagnetics: An Introduction' (Springer-Verlag, Inc., New York, NY, 2001)

50 Emerson and Cuming Microwave Products, Inc.: 'ECCOSORB® SF Thin, Flexible, Resonant Absorbers', (2007), URL http://www.eccosorb.com/Collateral/Documents/English-US/SF.pdf

51 Agilent Technologies, Inc.: 'Technical Specifications Agilent Techologies PNA Series Network Analyzers E8362B/C, E8363B/C, and E8364B/C' (2008), URL http://cp.literature.agilent.com/litweb/pdf/E8364-90031.pdf

52 Microwave Engineering Corporation: 'Double-Ridge and MEC Flatguide® Flanges and Waveguide', URL http://www.microwaveeng.com/catalog/t22d.pdf

53 Engen, G.F., Hoer, C.A.: 'Thru-reflect-line: an improved technique for calibrating the dual six-port automatic network analyzer', *IEEE Trans. Microw. Theory Tech.*, 1979, **27**, (12), pp. 987–993

54 Hyde, M.W., Havrilla, M.J., Bogle, M.J., Lehman, N.J.: 'Broadband characterization of materials using a dual-ridged waveguide', *IEEE Trans. Instrum. Meas.*, 2013, URL http://www.ieeexplore.ieee.org/xpl/articleDetails.jsp?arnumber=6553350

55 Baker-Jarvis, J., Vanzura, E., Kissick, W.: 'Improved technique for determining complex permittivity with the transmission/reflection method', *IEEE Trans. Microw. Theory Tech.*, 1990, **38**, (8), pp. 1096–1103

56 Hyde, M.W., Havrilla, M.J., Bogle, A.E.: 'A novel and simple technique for measuring low-loss materials using the two flanged waveguides measurement geometry', *Meas. Sci. Technol.*, 2011, **22**, (8), pp. 085704, URL http://www.stacks.iop.org/0957-0233/22/i = 8/a = 085704

doi: 10.1049/iet-smt.2013.0128